The influence of aeration and compressibility on slamming loads during cone water entry

M. Elhimer[a,*], N. Jacques[a], A. El Malki Alaoui[a], C. Gabillet[b]

[a] ENSTA Bretagne, FRE CNRS 3744, IRDL, 2 rue François Verny, F-29806, Brest CEDEX 9, France
[b] IRENav, Institut de Recherche de l'Ecole Navale, F-29240 Brest, France

A B S T R A C T

The problem of the impact between a rigid body and a gas-liquid mixture is relevant to various engineering applications, including the design of breakwaters and LNG containers. In the present study, the particular problem of the impact of a rigid cone upon the surface of an aerated liquid is investigated. Numerical simulations of water entry of cones with different deadrise angles (7° and 15°) were performed using an explicit finite element method. The air-water mixture is modelled as a homogeneous fluid with a specific equation of state. In addition, experimental tests of the impact of a cone with a deadrise angle of 7° on the surface of bubbly water were performed. The air volume fraction was measured prior to the impact tests using optical probes, and the instantaneous impact force on the cone was measured using strain gauges. The results highlight a significant reduction of the impact load with the increase of the air volume fraction. Moreover, the numerical results show that this reduction is also dependent on the impact velocity. This phenomenon is found to be related to the nonlinearity of the equation of state of the air-water mixture.

1. Introduction

Naval and offshore structures should withstand high loads due to fast and repeated impacts with the water free surface. The design of such structures requires information about the hydrodynamic forces arising during these impacts. Examples of water impact problems are the slamming of ships in heavy sea conditions (Kapsenberg, 2011) and the water landing of aerospace structures (Seddon and Moatamedi, 2006). In some cases, air bubbles can be entrapped in the liquid. As the speed of sound in a liquid is significantly reduced by aeration, compressibility effects can probably play a certain role in this situation.

An early theoretical study on hydrodynamic impacts was conducted by von Karman (1929) in order to compute the loading on seaplane floats during landing. By considering the momentum conservation before and after the impact, this author derived a formula for the force on a wedge during water entry. Wagner (1932) developed a more refined theory of water impact, still widely applied. The Wagner model is dedicated to bodies with small deadrise angles. It assumes that the flow is incompressible and potential, and the boundary conditions are linearized and imposed on the initial liquid free surface. By using the linearized Bernoulli equation, the pressure distribution on the wetted surface is obtained. The distribution of the pressure is singular at the boundary of the wetted surface. However, the singularity is integrable and the force acting on the body can be computed by integrating the pressure over the wetted surface.

Several extensions of the Wagner theory have been proposed to correct this singularity and to improve its predictive capabilities

* Corresponding author.
E-mail address: mehdi.elhimer@ensta-bretagne.org (M. Elhimer).

(Cointe and Armand, 1987; Korobkin, 2004; Zhao and Faltinsen, 1993). Wagner's theory and its extension provides analytical or semi-analytical models for both 2D and 3D geometries, and compares well with experiments and fully non-linear numerical simulations for impacting bodies with small deadrise angles, see e.g. (Korobkin and Malenica, 2016; Tassin et al., 2012, 2010).

Most of the theoretical works on the prediction of slamming loads assumed an incompressible fluid flow. However, in several cases, the effect of liquid compressibility cannot be neglected. For example, in the early stage of the impact of a blunt body, the wetted surface could expand at a velocity close to or larger than the speed of sound in the liquid (Carcaterra and Ciappi, 2000, 2004; Korobkin, 1992). Several theoretical studies were dedicated to the effect of compressibility on impact loads. A seminal work was carried out by Skalak and Feit (1966). During an impact, the expansion velocity of the wetted area is equal to or larger than[1]:

$$V_e = \frac{V_i}{\tan(\beta)} \tag{1}$$

where V_i is the velocity of the impacting body and β the deadrise angle. When β is small, the expansion velocity is significantly larger than the impact velocity, and may approach the sonic speed in the fluid. In this case, fluid compressibility must be taken into account in the computation of the impact force.

Using the acoustic theory, Skalak and Feit (1966) proposed a linearized model for water entry at constant velocity of a wedge in a compressible liquid. They developed a solution for the hydrodynamic force and the pressure distribution using the analogy with the stationary problem of a plane lifting surface at a small angle of attack. Poruchikov, (1973, 1974) considered the problem of the penetration of rigid cones and wedges into an inviscid compressible fluid. His analysis was also conducted within the acoustic framework and the problem was solved analytically when the expansion velocity is subsonic. He showed that the omission of the compressibility effect may lead to a significant overestimation of the impact force. The case of impacting bodies of arbitrary shape was considered by Kubenko and Gavrinlenko, (1986, 1987) and by Korobkin, (1992, 1994).

One of the main practical applications for which compressibility effects are important is related to the field of coastal engineering. Breakwaters are subject to high loads due to the impact of breaking waves. In this case, the compressibility of the liquid is enhanced due to the presence of entrapped air bubbles. It is well known that the compressibility of an aerated liquid is very much higher than that of the pure liquid and that the sonic speed in a diphasic mixture decreases rapidly with the gas volume fraction (or void fraction), see e.g. (Brennen, 2005). For instance, the presence of even two percent by volume of air bubbles in sea water causes a dramatic reduction of the speed of sound from about $1500m/s$ to less than $100m/s$. Experimental evidences of the effect of aeration on hydrodynamic pressures during wave impact were reported in several studies (Bredmose et al., 2009; Bullock et al., 2001, 2007; Hattori et al., 1994; Walkden, 1999).

Despite its practical importance, only few works were dedicated to the impact of solid bodies on aerated liquids. Indeed, the theoretical studies reported previously are based on the acoustic theory. This means that they assume that only small volume changes take place and that the liquid speed of sound is constant. It is questionable if the acoustic approximation can be applied to the slamming on aerated liquids. Indeed, the response of a liquid-gas mixture is generally nonlinear and because of the high compressibility of the gaseous phase, moderate pressure increases can lead to significant volume variations. The influence of constitutive nonlinearities is of particular importance for shock propagation problems (Brennen, 2005; Drumheller, 1998; Grandjean et al., 2012; van Wijngaarden, 1972). It is also likely that this phenomenon plays a certain role in slamming and impact flow problems of bubbly mixtures.

One of the first theoretical studies on this topic is due to Peregrine and Thais (1996) who considered the case of an air-water mixture rapidly filling a cavity. This flow configuration has similar features with flip-through phenomenon. Peregrine and Thais (1996) employed a nonlinear barotropic relation (equation of state) in order to model the air-water mixture. They obtained an analytical solution for the pressure and observed noticeable reductions of the maximum pressure due to aeration, even for small void fractions.

Dias et al. (2010) developed a numerical model for fast transient flows of gas-liquid mixtures. They also employed a two-fluid barotropic model to describe the compressibility of the biphasic mixture. The discretization of the governing equations is based on a second-order finite-volume scheme. They presented several simulations of impact-related flows of aerated liquids (dam break and drop impact problems). Another numerical model for biphasic mixtures was developed by Bredmose et al. (2009) in order to simulate aerated wave impacts. The model was applied to waves of varying height breaking against a vertical wall (configuration similar to the one investigated experimentally by Bullock et al. (2007)). The results showed that the compressible barotropic model can successfully reproduce the main characteristics of violent breaking-wave impacts observed in experiments.

To our best knowledge, the first slamming experiments with an aerated liquid was performed by Eroshin et al., (1980, 1984, 1988). These authors investigated the impact on bubbly water of disks and cones. The advantage of slamming tests is that they make it possible to control more easily the experimental conditions (in particular the void fraction), as compared to full-scale breaking wave impact experiments. The sound celerity in bubbly water was estimated by measuring the propagation velocity of disturbances near the free surface. These authors investigated experimentally the relationship between the maximal impact force and the Mach number. Their results suggest that the linear acoustic approximation agrees satisfactorily with the experimental results only at small values of the Mach number. For large Mach numbers, the acoustic approximation yields a noticeable underestimation of the

[1] $V_i/\tan(\beta)$ corresponds to the expansion velocity of the wetted surface only for supersonic impacts. Because in this case, the free surface of the liquid remains undeformed. For subsonic impacts, the expansion velocity of the wetted surface V_c is slightly larger than $V_i/\tan(\beta)$ because of the pill-up effect. In the incompressible limit, the expansion velocity of the wetted surface V_c is 28% larger than $V_i/\tan(\beta)$, according to the Wagner theory.

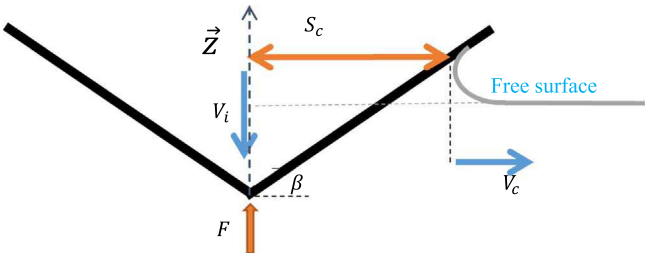

Fig. 1. Illustration of various quantities related to the cone entry problem.

maximal impact force. More recently, an experimental investigation was conducted by Walkden (1999), see also Bullock et al. (2001), in order to quantify the effects of aeration on wave impacts. A series of drop tests were conducted, in which a plate instrumented with pressure transducers impacted a tube filled with a bubbly liquid. In all cases, the maximum impact pressures were shown to decrease with increasing void fraction, especially for large impact velocities. It is worth noticing that, because the experiments of Walkden (1999) were conducted in a tube, they are not representative of water entry problems, but more of shock or flat impact problems.

The present work is aimed at quantifying the effects of the aeration on the hydrodynamic loads during the entry of bodies with a simple geometrical form, namely cones, in an air-water mixture. Numerical simulations and experiments were carried out. The numerical model is described in Sections 2.1 and 2.2. The considered impact problem was investigated using explicit finite element simulations. The air-water mixture behaviour is modelled using a non-linear equation of state. Section 2.3 is dedicated to the discussion of the numerical results and the analysis of the role played by aeration. In addition, experimental impact tests of a rigid cone on the surface of a bubbly liquid were performed using a large scale shock machine (El Malki Alaoui et al., 2012, 2015). The instantaneous impact force was measured using strain gauges. An array of porous soaker hoses was used for bubbles generation. The air volume fraction in the bubble plume was measured by optical probe technique. The experimental set-up and the instrumentation are described in Section 3.1. Finally, the experimental results are presented and compared to numerical results.

2. Numerical model and results

2.1. Numerical model

Finite element simulations of cone impact on the free surface of an air-water mixture were performed using the finite element software ABAQUS/Explicit. Explicit finite element computations were used previously by several authors for the modelling of impact flows (Aquelet et al., 2006; Federico and Amoruso, 2009; Wang and Guedes Soares, 2014), since they are well suited to simulate fast transient phenomena. The present numerical simulations are similar to those carried out in previous studies for the case of pure liquids (Jacques et al., 2010; Tassin et al., 2010; El Malki Alaoui et al., 2012). The readers may refer to these papers for more details.

The configuration considered in the simulations is illustrated in Fig. 1. The cone moves in the $\vec{z}$ direction with a constant velocity $-V_i.\ \vec{z}$. The cone radius was equal to 165 mm and two deadrise angles were considered: $\beta = 7°$ and $\beta = 15°$. The fluid was initially at rest. The impact velocity V_i was ranging between $0.\ 2$ m.s^{-1} and $170 m.s^{-1}$ for $\beta = 7°$ and between $0.\ 43 m.s^{-1}$ and $371 m.s^{-1}$ for $\beta = 15°$. The expansion velocity V_e was between $1.\ 62 m.s^{-1}$ and $1385 m.s^{-1}$ for both deadrise angles. The size of the fluid domain was equal to 2×2 m. Frictionless unilateral contact is used to describe the interaction between the fluid and the impacting solid.

The software ABAQUS/explicit uses by default a Lagrangian approach, where the mesh moves with the fluid motion. The drawback of this approach in the present case is that large deformations of the fluid take place in the impact region, leading to an excessive distortion of the mesh. In order to avoid this problem, the adaptive meshing technique of ABAQUS was employed. This method is based on an Arbitrary Euler-Lagrange (ALE) formalism, in which the mesh moves independently of the fluid flow, coupled with the operator-split technique (Souli et al., 2000). With the adaptive meshing procedure, a new mesh is created at a certain frequency, in order to reduce the distortion of the elements, and the solution variables (stress, density and velocity) are transferred from the old mesh to the new one.

In order to reduce the computational cost of the simulations, the ALE adaptive meshing technique was used only in the impact region, where large deformations are expected to occur. A Lagrangian mesh was used for the rest of the fluid domain, see Fig. 2. The ALE region was meshed using 110,250 axisymmetric 4-node elements with reduced-integration (ABAQUS CAX4R) with the same initial size. The Lagrangian domain was meshed with 68,398 axisymmetric 3-node linear elements (CAX3), with a mesh size increasing with the distance to the ALE region. The mesh size in the impact region was equal to 0.25 mm. We verified that using a finer mesh does influence the simulation results.

The ability of this numerical model to accurately predict slamming loads was assessed previously in the case of impacts on pure water from comparison with experiments (El Malki Alaoui et al., 2012; Jacques et al., 2010; Tassin et al., 2010). Moreover, a comparison with the analytical model of Poruchikov (1973) for the impact of a cone on a compressible (pure) liquid is presented in Appendix A. We also checked that ABAQUS is able to describe shock wave propagation in bubbly mixtures (as high velocity impacts cause the formation of a shock wave), see Appendix B.

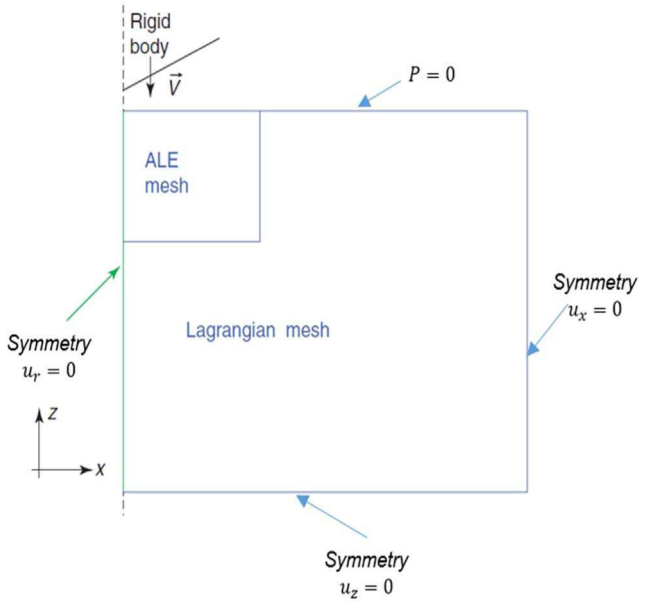

Fig. 2. Sketch of the computational model used in the present study.

2.2. Equation of state for aerated liquids

In the numerical model, aerated water is considered as a homogeneous mixture of a compressible liquid (pure water) and a compressible gas (air). Both phases are assumed to share locally the same pressure and velocity. These assumptions made in previous studies on impact flows of bubbly mixtures (Bredmose et al., 2009; Dias et al., 2010; Peregrine and Thais, 1996). Let us consider a Representative Volume Element (RVE) of the diphasic mixture and denote by V_L and V_G the volume of the parts of the RVE occupied by the liquid and by the gas, respectively. The total volume V of the RVE is given by $V=V_L + V_G$. The volume fraction of gas in the RVE or void fraction is defined as:

$$\alpha=\frac{V_G}{V} \tag{2}$$

Denoting by $\rho_G$and ρ_L the densities of the gas and liquid phases, respectively, the mixture density ρ can be expressed as:

$$\rho = \alpha\rho_G + (1 - \alpha)\rho_L \tag{3}$$

The effect of surface tension is neglected and we assume that the representative volume is in static equilibrium. This means that the individual dynamics of the bubbles are not considered in the present work. Therefore, the pressure is the same in the two phases: $P_L = P_G=P$. With this hypothesis, the air-water mixture can be regarded as a barotropic fluid having a unique pressure-density relationship.

Prior to the impact, the fluid is initially at the atmospheric pressure P_0. The initial volumes of the gas, the liquid and the mixture are referred to as V_{G0}, V_{L0} and V_0 respectively. The initial void fraction is referred to as α_0. The increase of the pressure causes a compaction of the RVE. It can be easily shown that the specific volume V/V_0 of the mixture is related to those of the gas and liquid phases by the equation:

$$\frac{V}{V_0} = \alpha_0\frac{V_G}{V_{G0}} + (1-\alpha_0)\frac{V_L}{V_{L0}} \tag{4}$$

The two terms of the right hand side of the equation can be expressed from the equation of state of each phase. The air is considered as an ideal gas undergoing an isentropic compression. The air specific volume is related to the pressure P using Laplace's law:

$$\frac{V_G}{V_{G0}} = \left(\frac{P}{P_0}\right)^{-1/\gamma} \tag{5}$$

where γ is the Laplace coefficient. γ=1 corresponds to isothermal conditions, while γ=1.4 (for air) to adiabatic conditions. It is not clear if isothermal or adiabatic conditions dominate for water impact problems. For the applications considered here, the typical bubble radius is between 0.1 and 1 mm. For bubbles in this size range, the time necessary to reach thermal equilibrium after compression is between some tenths of milliseconds and some milliseconds (but significant heat exchanges with the liquid take place at shorter times) (Kameda et al., 1998; Watanabe and Prosperetti, 1994). This time can be smaller or larger than the duration of an

impact depending on the impact velocity. All the results presented in the present paper were obtained with γ=1. We also carried out some simulations for γ=1.4. The results of these simulations were very close to those obtained with γ=1. Peregrine and Thais (1996) also investigated the effect of the polytropic index and also concluded that the value of γ has only a minor effect on the loads generated during an impact on an air-water mixture.

The water phase is considered as a weakly compressible media, where the volume change is related to the pressure through a linear[2] equation of state:

$$\frac{V_L}{V_{L0}} = \left(\frac{P-P_0}{K_{L0}}+1\right)^{-1} \tag{6}$$

where K_{L0}=2. 19GPa is the water bulk modulus.[3] Finally, we obtain the following equation of state for the two phase mixture:

$$\frac{V}{V_0} = \alpha_0\left(\frac{P}{P_0}\right)^{-1/\gamma} + (1-\alpha_0)\left(\frac{P-P_0}{K_{L0}}+1\right)^{-1} \tag{7}$$

Because of the difference of compressibility between the gas and liquid phases, a compression of the mixture leads to a decrease of the void fraction. The current value of void fraction in the mixture can be expressed as a function of the pressure (see Appendix C):

$$\alpha = \frac{\alpha_0(P/P_0)^{-1/\gamma}}{\alpha_0(P/P_0)^{-1/\gamma} + (1-\alpha_0)\left(\frac{P-P_0}{K_{L0}}+1\right)^{-1}} \tag{8}$$

Fig. 3 shows the variation of the specific volume as a function of the pressure for air-water mixtures for different initial void fractions: α_0=1%, 5% and 10%. Fig. 4 presents the evolution of the void fraction α with the pressure for the same initial values of void fraction. From these figures, three different stages can be distinguished depending on the pressure value. The variation of the specific volume and the void fraction is negligible for relative pressure below 10^4Pa. Indeed, for $P-P_0 < 10^4$Pa, the value of V/V_0 remains close to unity and α remains close to its initial value α_0. The effects of the mixture compressibility become noticeable for larger pressures. For $P-P_0$ ranging between 10^4Pa and 10^7Pa, the ratio V/V_0 decreases with the pressure and eventually reaches a value close to $1-\alpha_0$. This is concomitant with a sharp decrease of the void fraction, which becomes negligible in comparison with its initial value. On the other hand, the water volume change is negligible (the ratio V_L/V_{L0} remains close to unity). Therefore, the change of the specific volume in this range of pressure results only from the air compressibility. For larger pressures, $P-P_0 > 10^7$, the specific volume decreases more rapidly. The air volumetric fraction is very small and therefore the volume change of the mixture is mainly due to the volume change of the water phase.

Let us now examine the evolution of the acoustic properties of air-water mixtures during compression. The sonic speed is defined as (Brennen, 2005):

$$c = \left(\frac{\partial P}{\partial \rho}\right)^{1/2} \tag{9}$$

From the equation of state (7), the following expression of the sound speed for a diphasic mixture as a function of the void fraction can be derived (Brennen, 2005):

$$\frac{1}{c^2} = (\alpha\rho_G + (1-\alpha)\rho_L)\left(\frac{\alpha}{\rho_G c_G^2} + \frac{1-\alpha}{\rho_L c_L^2}\right) \tag{10}$$

where c_G and c_L are respectively the speed of sound in pure air and in pure water at the considered pressure, $c_G = \sqrt{\gamma P/\rho_G}$ and $c_L = \sqrt{K_{L0}/\rho_{L0}}$. Fig. 5 shows the evolution of the sound speed c as a function of the pressure for several initial values of void fraction. For pressures up to 10^4Pa, the speed of sound remains almost constant because the void fraction and the phase sonic speeds are nearly unchanged. For larger pressures, the sonic speed increases gradually as an effect of the decrease of the void fraction and the increase of the gas sound speed. At very large pressure, c becomes close to the sonic speed of the liquid phase, as the void fraction tends towards zero. Thus, as an impact may involve large increases of pressure in the fluid, the void fraction and the sound speed may change significantly in the impact region.

In ABAQUS/Explicit, the equation of state was specified in tabular form as a relation between $P-P_0$ and $\ln(V/V_0)$. The values of initial void fraction considered in the simulations were α_0=1%, α_0=5% and α_0=10%, in addition to the case of pure water α_0=0. As it will be shown hereafter, these void fractions are large enough to have a significant effect on the impact loads and pressures.

[2] With this equation of state, the liquid density ρ_L is a linear function of the pressure.

[3] At 20°C and atmospheric pressure, the speed of sound in water c_{L0} is equal to $1481 m/s$(Wilson, 1959) and the water density ρ_{L0} is equal to $997 kg/m^3$. From these values, the bulk modulus for water is calculated using the following relation: $K_{L0} = \rho_{L0} c_{L0}^2$=2. 19GPa.

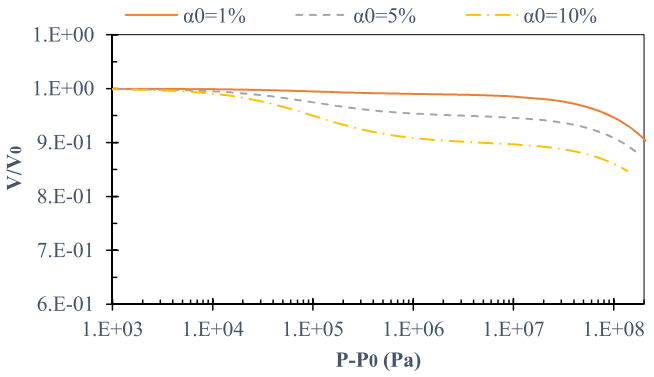

Fig. 3. Evolution of the specific volume V/V_0 as a function of the pressure for three initial void fractions α_0, as predicted by the two-phase equation of state (see Section 2.2).

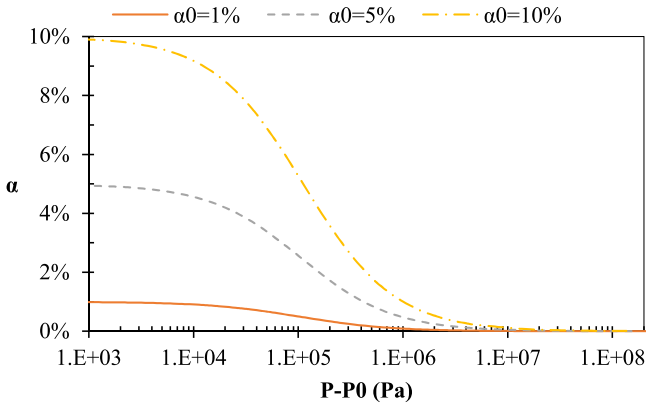

Fig. 4. Void fraction α as a function of the pressure for three initial void fractions α_0, as predicted by the two-phase equation of state (see Section 2.2).

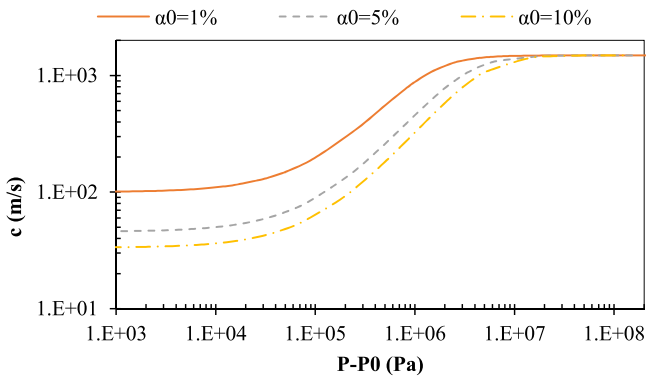

Fig. 5. Sonic speed in the mixture c as a function of the pressure for three initial void fractions α_0, as predicted by the two-phase equation of state (see Section 2.2).

2.3. Numerical results

2.3.1. Effect of aeration on impact force, pressure and wetted surface

Let us introduce some notations that will be used in the next sections of this paper. The ensemble of the nodes in contact with the cone defines the contact surface and its area is noted S_c. The impact force F is obtained by summing the vertical components of the contact forces on all nodes of the contact surface. The average pressure acting on the contact surface is given by $P_m = F/(S_c.\cos(\beta))$.

Time evolutions of the impact force for a deadrise angle of 7°, an impact velocity of 10 m/s and several initial void fractions (α_0=1%,5% and 10%) are shown in Fig. 6. In all cases, F is proportional to t^2 (this behaviour is consistent with dimensional analysis, see Section 2.3.2). By comparing the different curves, it is observed that the force at a given time decreases significantly with the initial void fraction α_0, highlighting the reduction of the impact force due to aeration. Since both F and S_c vary as t^2, the average pressure P_m is constant during the cone impact. In Fig. 7, P_m is presented as a function of the expansion velocity V_e for all void fractions and deadrise angles. It is showed that the average pressure is reduced when α_0 increases.

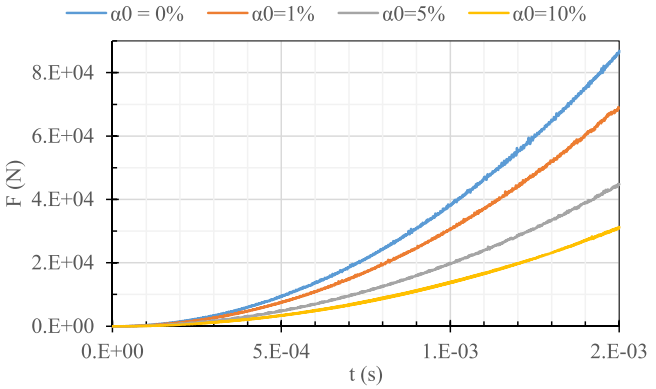

Fig. 6. Time evolution of the impact force from ABAQUS/Explicit simulations for pure water (α_0=0%) and aerated water (α_0=1%, α_0=5%, α_0=10%). The impact velocity is V_i=10 $m.s^{-1}$.

In order to analyse the combined effect of the impact velocity and the initial void fraction on the slamming load, we calculated the ratio between the impact force F_α for a given initial void fraction α_0 and the impact force F_0 for the pure liquid, at the same impact velocity V_i and penetration depth (it should be noted that this ratio does not depend on the penetration depth as both F_0 and F_α are proportional to t^2). This ratio is referred to as the force reduction factor (FRF).

Fig. 8 shows for both deadrise angles (β=7° and β=15°) the evolution of the force reduction factor F_α/F_0 as a function of the expansion velocity V_e. One observes that aeration leads to a reduction of the impact force for any value of V_e, since the FRF is always smaller than unity and the FRF decreases with the initial void fraction. Interestingly, these results highlight the dependence between the impact velocity and the force reduction due to the aeration. Indeed, the FRF is velocity dependent for all void fractions. The

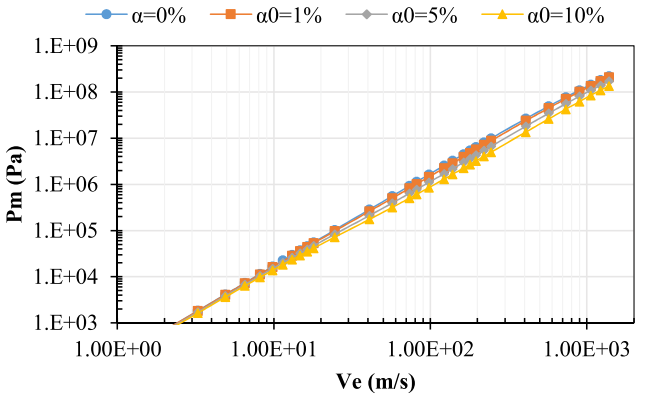

a)

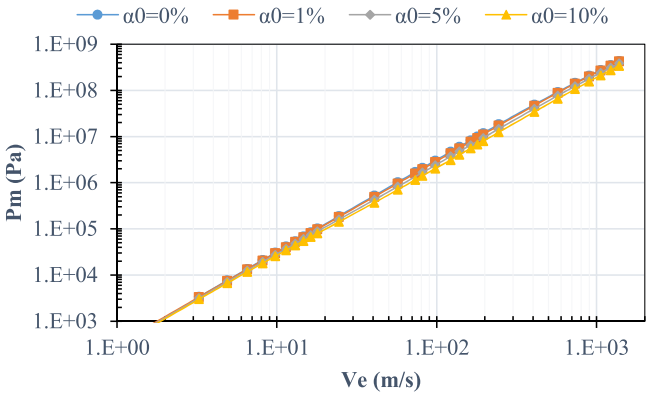

b)

Fig. 7. Evolution of the average impact pressure as a function of the expansion velocity V_e. Results from ABAQUS/Explicit simulations for pure water (α_0=0%) and aerated water (α_0=1%, α_0=5%, α_0=10%). a) Deadrise angle β=7°, b) β=15°.

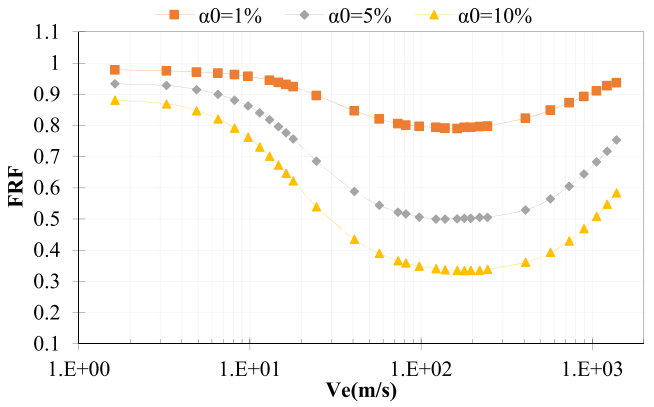

a) $\beta = 7°$

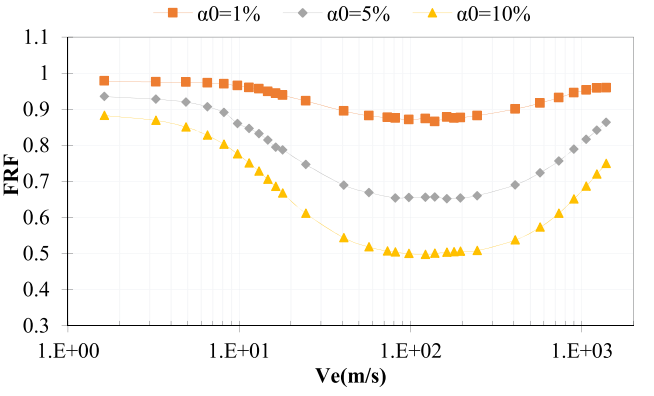

b) $\beta = 15°$

Fig. 8. Force reduction factor F_α/F_0 (from ABAQUS/Explicit simulations) as a function of the expansion velocity V_e for three void fractions α_0=1%, α_0=5% and α_0=10%. a) deadrise angle β=7°, b) deadrise angle β=15°.

largest force reductions are observed for expansion velocities V_e ranging between $100m.s^{-1}$ and $300m.s^{-1}$. For β=7°, this corresponds to impact velocities V_i between 12 $m.s^{-1}$ and 36 $m.s^{-1}$, these values can be encountered in several applications and can be achieved in experiments.

For low-velocity impacts, $V_e < 5m.\ s^{-1}$, the FRF is equal to the ratio of the initial mass density of the aerated mixture and the one of the liquid, $F_\alpha/F_0 \approx \rho_{\alpha 0}/\rho_{L0}$. For these velocities, our simulations show that the average impact pressure P_m is lower than 10^4Pa, see Fig. 7. Therefore, in this case, the impact does not cause a significant change of the volume of the bubbly mixture, see Fig. 3. Consequently, the fluid flow is isochoric and the force reduction due to aeration is only related to the decrease of the initial mass density of the mixture.

At larger velocities, the influence of the enhanced compressibility of the bubbly mixture becomes significant and smaller values of FRF are observed. For example, with β=7° and V_i=30 $m.s^{-1}$ (V_e=244 $m.s^{-1}$), a load reduction of about 67% ($F_\alpha/F_0 \approx 0.33$) is observed for an initial void fraction of α_0=10%. Even for a small void fraction of 1%, a maximum load reduction of about 20% ($F_\alpha/F_0 \approx 0.8$) is achieved. The force reductions observed with the deadrise angle β = 15° are smaller, but remains significant. For very high velocity impacts ($V_e > 300m.s^{-1}$), the FRF increases with the impact velocity. This phenomenon is caused by the reduction of the void fraction induced by the impact. Indeed, when $V_e > 300m/s$, the average impact pressure P_m is larger than 10^7Pa, so the air volume fraction in the impact region become negligible (see Fig. 4). Therefore, the effect of aeration on the load is reduced and the influence of the water compressibility prevails.

We now turn our attention to the reduction of the average pressure due to the aeration. We define the pressure reduction factor (PRF) as $P_{m\alpha}/P_{m0}$ where $P_{m\alpha}$ is the average pressure for an initial void fraction α_0, and P_{m0} is the average pressure for pure water, at the same impact velocity and penetration depth. Fig. 9 displays the evolution of the PRF with the expansion velocity V_e for the three initial void fractions and the two deadrise angles considered. The evolution of the PRF with V_e exhibits the same trends as for the FRF. Indeed, for small impact velocities, the PRF is close to the density ratio $\rho_{\alpha 0}/\rho_{L0}$, meaning that the pressure reduction is only due to the decrease in mass density caused by the presence of the gas phase. At larger velocities, $Ve>5m/s$, the PRF decreases with the expansion velocity and reaches a minimum for V_e close to $150m/s$, for all values of initial void fraction and deadrise angles considered. For α_0=5%, the minimum of the PRF is equal to 0.66 for β=7° and to 0.78 for β=15°.

Interestingly, the reduction of the average pressure is smaller than the force reduction for the same expansion velocity. For

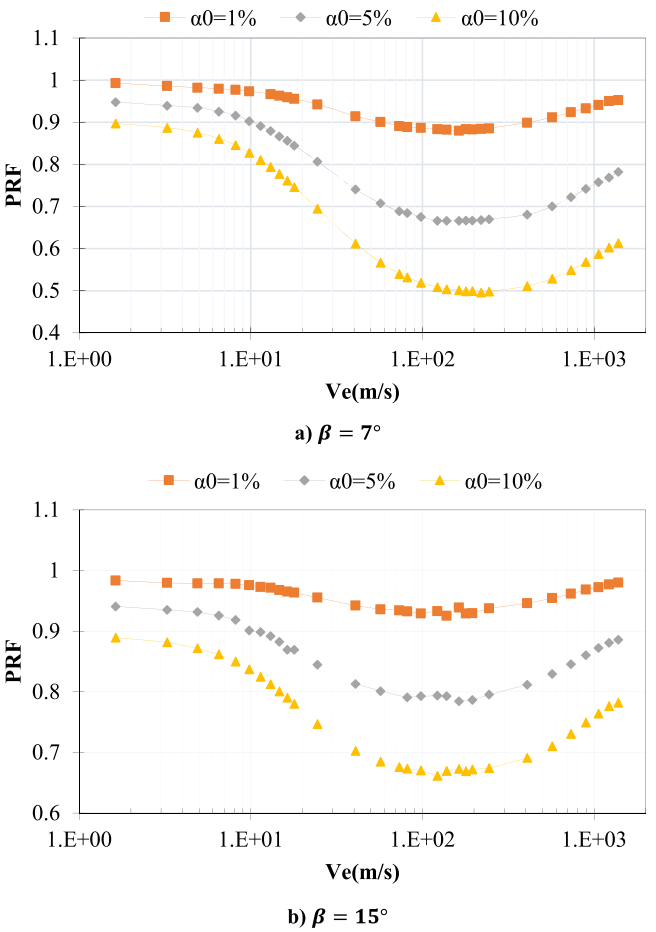

Fig. 9. Average pressure reduction factor $P_{m\alpha}/P_{m0}$ (from ABAQUS/Explicit simulations) as a function of the expansion velocity V_e for three void fractions α_0=1%, α_0=5% and α_0=10%. a) deadrise angle β=7°, b) deadrise angle β=15°.

example, with β=7°and α_0=10%, the minimum value of the FRF is equal to 0. 33, while the minimum PRF is only of 0. 5. This suggests that the surface contact area S_c (for a given impact velocity and penetration depth) is also affected by aeration.

In order to evaluate this effect, we computed the ratio $S_{c\alpha}/S_{c0}$ where $S_{c\alpha}$ is the contact surface for an initial void fraction α_0 and S_{c0} is the contact surface for pure water, at the same impact velocity and penetration depth. This ratio will be referred to as the contact area reduction factor (CARF) in the following. The evolution of the CARF with V_e is presented in Fig. 10. These results show that aeration may induce a significant reduction of the contact surface area, depending on the impact velocity. For very small velocities, $V_e < 5m/s$, the CARF is close to unity. This means that aeration does not affect the size of the wetted surface for this range of velocities and therefore the PRF and FRF are close (they are almost equal to the density ratio $\rho_{\alpha 0}/\rho_{L0}$).

The reduction of the contact surface due to aeration is noticeable for a large range of intermediate velocities, $10m/s < V_e < 1000m/s$. Even for a small initial void fraction of 1%, the maximum reduction of the surface area is of 10% for β=7° and of 6% for β=15°. The reduction of the contact surface is higher for α_0 = 10% as it reaches 33% for β=7° and 25% for β=15°. Since FRF = PRF × CARF, the difference between the PRF and the FRF is maximal for expansion velocities around 150m/s, when the CARF reaches its minimum.

At larger velocities, the CARF increases and tends towards 1 when V_e becomes close to the speed of sound of the liquid phase. In this case, the impact is supersonic: the liquid free surface remains undisturbed during the entry of the cone, see e.g. (Skalak and Feit, 1966). It is worth noticing that, according to our simulations, the supersonic impact regime for an aerated mixture does not take place when the expansion velocity reaches the value of the initial sonic speed of the mixture (see Eq. (10)), but the value of the speed of sound of the water. This phenomenon can be understood by considering the results presented in Figs. 4, 5 and 7. The large pressures generated during high velocity impacts cause a strong reduction of the air volume fraction in the impact region and an increase of the speed of sound in the mixture. That is the reason why the supersonic regime, i.e. when the free surface is undisturbed during the impact, is reached only for expansion velocities approaching the speed of sound of the liquid phase.

More insights into pressure and contact surface reduction can be gained from the pressure on the cone surface. Fig. 11 displays the pressure distribution acting on a cone with a deadrise angle of 7° for several values of the initial void fraction (α_0=0%, α_0=1%, α_0=5% and α_0=10%) and an impact velocity of 10 m/s. For these impact conditions, corresponding to V_e=81.5m/s, the reductions of

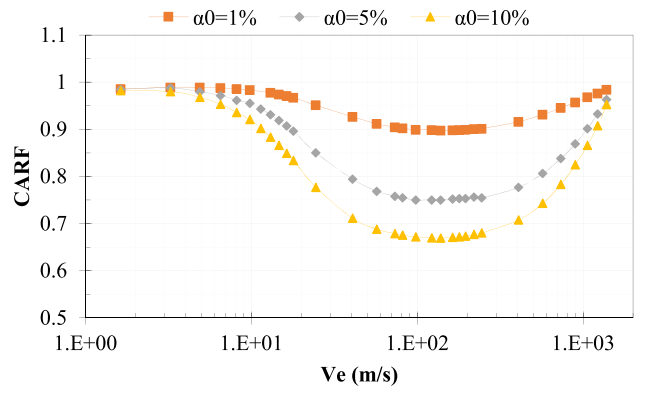

a) $\beta = 7°$

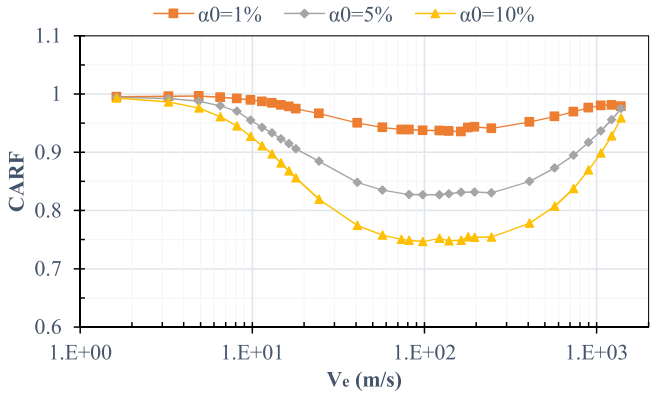

b) $\beta = 15°$

Fig. 10. Contact surface reduction factor ***CARF*** (from ABAQUS/Explicit simulations) as a function the expansion velocity V_e for three void fractionsα_0=1%, α_0=5% and α_0=10%. a) deadrise angle β=7°, b) deadrise angle β=15°.

the force, average pressure and contact surface area due to aeration are significant and close to their minima, see Figs. 8 and 9. Fig. 11 shows that, for all void fractions, the pressure distribution is highly heterogeneous. The pressure increases strongly near the boundary of the contact surface. It is observed that the peak pressure decreases with the initial void fraction. It is interesting to notice that the ratio between the peak pressure P_{max} and the average pressure P_m does not depend very much on the value of the initial void fraction, see Table 1. This indicates that the reduction of the peak pressure caused by aeration is similar to the reduction of the average pressure. In Fig. 11, the reduction of the surface contact area due to aeration discussed previously is also visible. In the case of an impact on an incompressible liquid, the peak pressure is proportional to $\rho_0 V_c^2$, with V_c the expansion velocity of the surface contact, see (Cointe and Armand, 1987; Zhao and Faltinsen, 1993). Table 1 presents the values of $2P_{max}/\rho_0 V_c^2$ for the four initial void

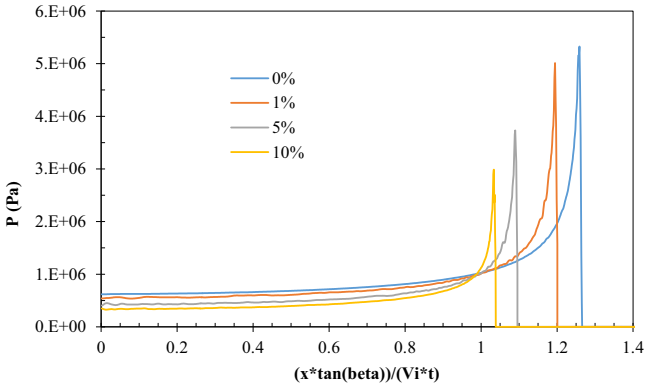

Fig. 11. Pressure distribution on the cone surface for an impact velocity of 10 m/s and a deadrise angle of 7° (corresponding to V_e=*81. 5m/s*). Four different initial void fractions are considered: α_0=*0* (pure water), α_0=*1*%, α_0=*5*% and α_0=*10*%.

Table 1
Characteristic values of the pressure distributions plotted in Fig. 11. V_c is the surface contact expansion velocity, P_m is the average pressure and P_{max} is the peak pressure.

α_0	V_c(m/s)	P_m(kPa)	P_{max}(kPa)	P_{max}/P_m	$2P_{max}/\rho_0 V_c^2$
0	103	1155	5325	4.61	1
1%	98	1032	5013	4.86	1.06
5%	89	787	3732	4.74	0.99
10%	85	616	2986	4.84	0.93

fractions considered. It is seen that these quantities are almost constant. This suggests that the reduction of the peak pressure is directly related to the reduction of the surface contact expansion velocity in the present case."

2.3.2. Dimensional analysis and dimensionless numbers relevant to the problem

The aim of the present section is to identify the physical parameters that control the load reduction during a cone impact on an aerated fluid. To that purpose a dimensional analysis of the present problem was performed. A special attention was accorded to the dependence of the slamming force with respect to the parameters that define the behaviour of the air-water mixture and the impact conditions (introduced in Sections 2.1 and 2.2):

$$F = \Pi(V_i,\ t,\ \beta,\ \alpha_0,\ \rho_0,\ P_0,\ K_L,\ \gamma) \tag{11}$$

Using the Vashy-Buckingham theorem, it is possible to define six dimensionless numbers from these nine physical variables. The choice of dimensionless numbers is not unique. In the present case, the following numbers were chosen:

$$f = \Pi^*\left(M,\ \beta, \alpha_0,\ \frac{P_0\gamma}{K_L}, \gamma\right) \tag{12}$$

The first one is the slamming coefficient f defined as (El Malki Alaoui et al., 2012; Shiffman and Spencer, 1951) :

$$f = \frac{F\tan^3(\beta)}{\rho_0 V_i^4 t^2} \tag{13}$$

For an incompressible impact, the slamming coefficient depends only on the deadrise angle, $f=\Pi^*(\beta)$. So the impact force scales with time and impact velocity as $F\sim t^2$ and $F\sim V_i^4$. El Malki Alaoui et al. (2012) found experimentally the following values $f(7°)=6.\ 79$ and $f(15°)=6.\ 18$.

The second dimensionless number is the Edge Mach number M, introduced by Skalak and Feit (1966) in their theoretical study of wedge impacts on compressible liquids:

$$M = \frac{V_e}{c_0} \tag{14}$$

V_e is the expansion velocity, related to the impact velocity by Eq. (1), and c_0 is the initial speed of sound in the air-water mixture given by Eq. (10) (considering the initial void fraction α_0 and the initial pressure P_0). The values of c_0 for the initial void fractions considered in the present simulations are provided in Table 2.

The other dimensionless numbers are the deadrise angle β, the initial void fraction α_0, the ratio of the initial bulk modulus of the gas phase to the one of the liquid phase $P_0\gamma/K_{L0}$ and the Laplace coefficient γ. In the present study, the attention was focused on air-water mixtures. Therefore, the influence of the two last numbers was not investigated.

Fig. 12 presents the evolution of the slamming coefficient f with the edge Mach number M for several values of the initial void fraction and two different deadrise angles. Let us first examine the case of the pure liquid ($\alpha_0=0$). Two different impact regimes can be identified. For very low values of Mach number, $M<0.05$, the slamming coefficient is almost constant, meaning that the effect of liquid compressibility is negligible. At larger Mach numbers, a gradual decrease of the slamming coefficient is observed. Moreover, the slope of the curve $f - \ln(M)$ decreases monotonically when the Mach number increases. The value of f when M is tending towards 1 is about two times smaller than the value corresponding to the incompressible regime for both deadrise angles.

The evolution of the slamming coefficient with the Mach number is more complex for an air-water mixture. At low Mach numbers, the evolution of f is identical to the one observed for a pure liquid. The incompressible regime, where f is constant, also takes place for values of M lower than 0.05. (However, it should be noted that this corresponds to much lower impact velocities for an aerated liquid. For instance, with $\alpha_0=1\%$ and $\beta = 7°$, $M = 0.\ 05$ is obtained for an impact velocity of only 0.62 m/s). For $M>0.05$,

Table 2
Values of the sonic speed at atmospheric pressure in an air-water mixture for the initial void fractions considered in the present study.

α_0(%)	0%	1%	5%	10%
c_0(m.s^{-1})	1481	100. 4	45. 9	33.3

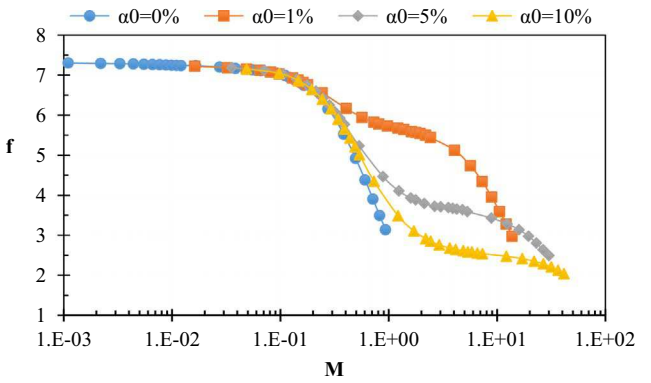

a) $\boldsymbol{\beta} = 7°$

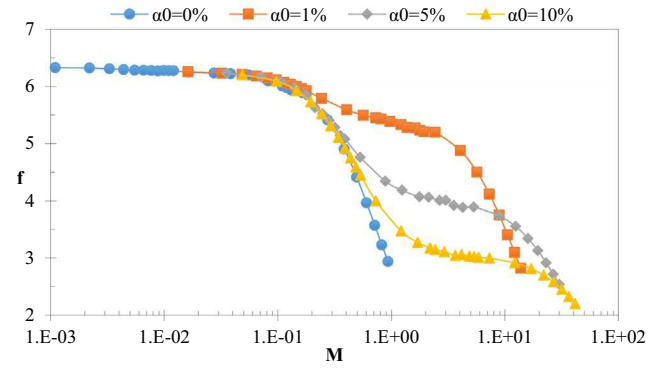

b) $\boldsymbol{\beta} = 15°$

Fig. 12. Evolution of the slamming coefficient **f** (from ABAQUS/Explicit simulations) as a function of the edge Mach number $\mathbf{M=V_e/c_0}$ for aerated liquids with different initial void fractions $\boldsymbol{\alpha_0}$ and for pure water ($\boldsymbol{\alpha_0=0}$%). a) deadrise angle $\boldsymbol{\beta} = 7°$, b) $\boldsymbol{\beta} = 15°$.

the influence of compressibility becomes significant and f decreases with the Mach number. At the beginning, the evolution of f is similar to that for the pure liquid. Nevertheless, when M goes beyond 0.3, the relation between f and M becomes dependent of the initial void fraction. In particular, we observe that for an aerated mixture there is a range of Mach number for which f remains fairly constant. For instance, with α_0=1% and $\beta = 7°$, the slamming coefficient only decrease from 5.82 to 5.44 for $0.73 < M < 2.43$. Then, f decreases rapidly for larger Mach numbers. This phenomenon is thought to be related to the nonlinearity of the equation of state of the aerated water and the decrease of the air volume fraction due to the large pressures generated by the impact. Indeed, we observed that the values of the Mach number where the evolution of f with M for the aerated liquids depart from the one for pure water corresponds to impact pressures for which the void fraction begins to drop rapidly, see Fig. 4.

From the results displayed in Fig. 12, it appears that the reduction of slamming loads due to aeration cannot be interpreted by considering only the influence of the void fraction on the initial bulk modulus (or sonic speed) of the mixture, as the slamming coefficient generally depends on the Mach number **and** the initial void fraction. A proper analysis of the influence of aeration on slamming loads requires the use of a nonlinear equation of state.

3. Experimental methods and results

3.1. Experimental set-up and methods

3.1.1. Description of the experimental set-up and instrumentation

Impact tests on aerated water were conducted using the SERVOTEST hydraulic shock machine of ENSTA Bretagne, with a large water tank underneath (Fig. 13). The tank was $2m$ wide, $3m$ long and $2m$ deep, and was filled with water to a height of 1.2 m. An aluminum cone with a deadrise angle of 7° and a diameter of 33cm was screwed at the end of the machine piston (Fig. 14). The instrumentation was similar to the one used in previous studies (El Malki Alaoui et al., 2012, 2015). A set of twelve strain gauges was mounted near the piston end. These gauges measured the force acting on the cone. Moreover, a piezo-resistive accelerometer was mounted on the cone to measure its acceleration during the tests and an internal sensor of the machine provided the position of the piston. A differential acquisition system recorded the signals at a frequency of 100kHz. Based on the devices sensitivity, the uncertainty on the force measurements is estimated at $\pm 10^3 N$ and the uncertainty on the acceleration measurements is estimated at $\pm 0.12g$.

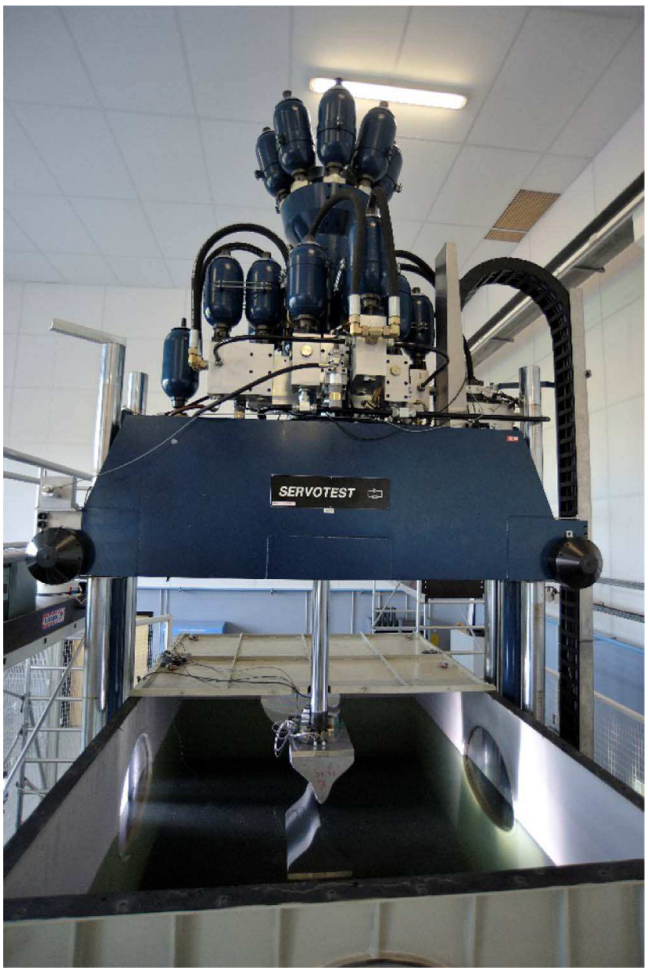

Fig. 13. The hydraulic shock machine used for the experimental impact tests. The water tank is underneath the shock machine. The cone is not shown on this picture.

The shock machine is able to maintain the translation velocity of the piston almost constant during the impact stage. For the impact tests reported in this paper, the reference impact velocity was set to V_i=8m/s . The cone velocity V_i was computed by integration of the acceleration signal. It was observed that the cone velocity was within ±4% of the reference velocity for all tests. The cone vertical position z was computed from the integration of the velocity signal, and checked against the values given by the machine displacement sensor (see El Malki Alaoui et al., 2012, 2015).

The total force F_{tot} is the sum of the inertial force m. a and the hydrodynamic impact force F applied on the cone:

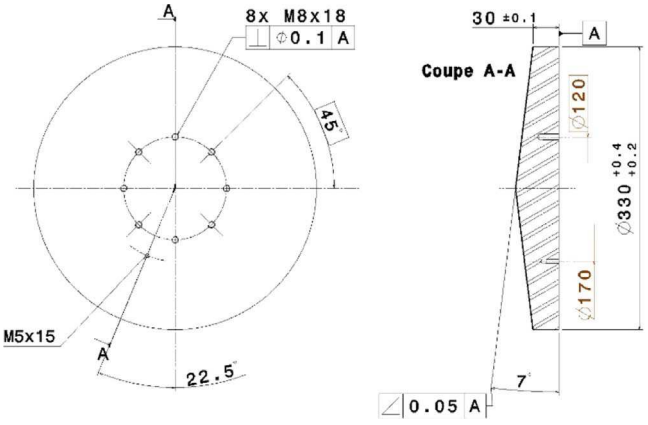

Fig. 14. Dimensions of the aluminium cone used in the experiments.

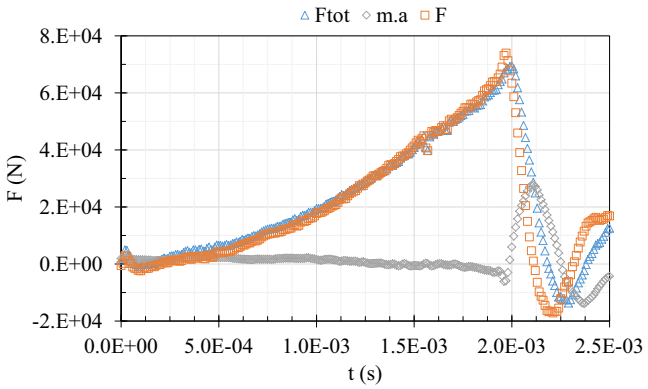

Fig. 15. Example of the recorded force signals during an impact test on pure water. $\mathbf{F_{tot}}$ is the total force measured by strain gauges **F** is the hydrodynamic impact force and **m**. **a** is the inertial force.

$$F=F_{tot}-m.\ a \tag{15}$$

The mass of the cone m is equal to 14kg. An example of force signals is shown in Fig. 15. The duration of the impact is of $2.\ 10^{-3}$s. At the end, the impact force F reaches 70kN while the inertial force ma was less than 6kN during the impact tests. After the full immersion of the cone, the hydrodynamic force drops when the flow separate from the cone (Peseux et al., 2005; Tassin et al., 2014).

For the purpose of air bubble generation, an aerator was put in the bottom of the water tank. It was made of an array of 30 parallel porous soaker hoses (Fig. 16). The hoses are $1.\ 3m$ in length and the array spans the width of the tank. Compressed air was injected at both ends of each hose. The total air mass flow rate was monitored using two rotameters connected in parallel. The injection pressure was controlled using a pressure regulator and measured by a digital manometer. According to Darcy's law, the flow rate through a porous medium is proportional to the pressure drop across the medium. We carried out several flow rate measurements for different injection pressures and checked that the flow rate increased linearly with the pressure. The impact tests reported in the present study were performed for three different values of the air mass flow rate Q, given in standard liter per minute (L_{std}/min) in Table 3. The uncertainty on the mass flow rate is estimated at $\pm\ \ 2.\ 5L_{std}$/min while the uncertainty on the air pressure is estimated at $\pm 0.\ 01$bar.

3.1.2. Void fraction measurement method

Prior to the impact tests, measurements of void fraction in the impact area were conducted using a single optical probe system (Barrau et al., 1999; Mäkiharju et al., 2013), build by RBI-Instrumentation. The optical probe was made of an optical fiber with a diameter of 10μm. The probe tip was immersed at different positions in the air-water mixture. An optical signal was generated by an optoelectronic module and injected into the fiber. The optical signal is completely reflected back to the optoelectronic module only when the tip is immersed in air (dewetted). This signal is converted to a voltage signal by the optoelectronic module and recorded by a NI acquisition card with a sampling frequency of 20KHz. This signal is then binarized in order to get the air characteristic function χ. When the voltage is larger than a user defined threshold, the probe tip is considered to be in contact with air, thus $\chi = 1$. Otherwise, when the voltage is lower than the threshold, the tip is considered to be wetted and $\chi = 0$. The void fraction is defined as

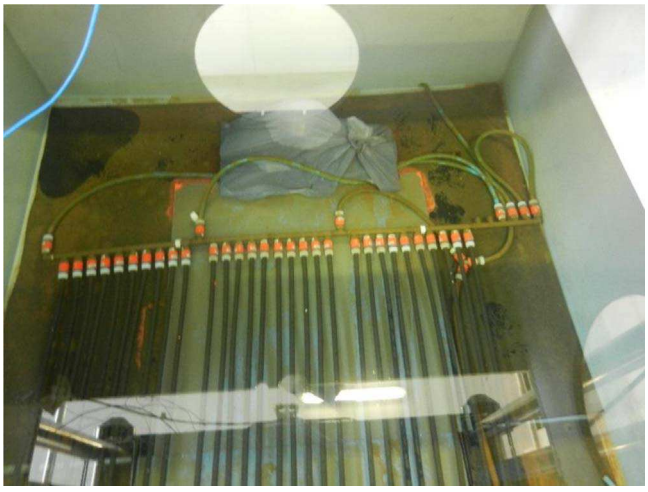

Fig. 16. Picture of the air bubble generator: an array of porous soaker hoses (black) at the bottom of the water tank.

Table 3
Air mass flow rate through the aerator as a function of the injection pressure.

Air injection pressure P(mBar)	1231	1345	1680
Air mass flow rate Q(L_{std}/min)	108. 3	174. 6	327

the time average of the air characteristic function over the acquisition time T:

$$\alpha_0 = \frac{1}{T}\int_0^T \chi(t)dt \tag{16}$$

In our measurements, the threshold was set to 10% of the voltage maxima. When the threshold is larger than the noise level, the measurement results are shown to be very little sensitive to the threshold. Indeed, the increase of the threshold from 10% to 50% of the maxima leads to a decrease of about 10% of the measured void fraction. The acquisition duration was 150 s and the acquisition was repeated three times. A mechanical device was used to translate the probe tip in two directions. The void fraction measurements were made at three horizontal positions Y = 16cm, Y = 0 and Y = − 16cm(Y = 0 corresponds to the axis of the piston machine), and four vertical positions Z = 0, Z = 10mm, Z = 20mm and Z = 50mm (the Z axis is oriented downward and Z = 0 corresponds to the position of the water free surface when no air is injected).

3.2. Experimental results

3.2.1. Void fraction measurements results

Vertical profiles of void fraction are presented in Fig. 17 for the three air flow rates considered.. As expected, the void fraction at any position increases with the air mass flow rate. For a given air mass flow rate, the relative difference between the minimal and maximal void fraction α_0 at the different measurement positions varies between 37% for Q = 108. 3 L_{std}/min and 13% for Q = 174. 6 L_{std}/min. The average values of α_0 for each mass flow rate are given in Table 4. The mean void fraction was ranging between 0. 35% and 1. 1%.

It can be observed that the mean void fraction increases linearly with the air mass flow rate. This suggests that the mean rising velocity of the bubbles was not sensitive to the air mass flow rate. Taking into account the size of the aerator, the estimated value of the average rising velocity of the bubbles is between 19cm.s^{-1} and 20cm.s^{-1}. This value corresponds to the terminal velocity of a single spherical bubble of diameter close to 1. 3mm rising in still water (Batchelor, 1967). This estimation of the bubble size is in good agreement with measurements performed with a small-scale aerator, made of the same porous soaker houses, in a smaller water tank using a double optical probes system. Indeed, these measurements showed that the bubble size was ranging between 1mm and 2mm (Croci et al., 2014). It should be observed that the rising velocity is very small compared to the impact velocity.

3.2.2. Impact force measurements results

Thirteen impact tests were carried out for an impact velocity V_i=8m/s: 2 for pure water, 5 for α_0=0. 35%, 3 for α_0=0. 56% and 3 for α_0=1. 1%. The results of the tests are presented in Fig. 18. For each test, the evolution of the impact force is plotted as a function of the cone position $z-z_s$ (z_s being the position of the cone at the time of full immersion, i.e. when the hydrodynamic force reaches its maximum). In previous studies (El Malki Alaoui et al., 2012, 2015), it was showed force measurements during impact tests on pure water are well repeatable. This is also visible in Fig. 18-a. Indeed, the results of the two tests for α_0=0% are very close. With aeration, a larger scatter between the results of different tests performed for the same air mass flow rate is observed. Most probably, this scatter is due to the unsteadiness of the bubbly flow. Indeed, it is well known that buoyancy-driven flows in bubble plumes are generally unsteady and turbulent, leading to the inhomogeneity of the void fraction distribution (Buwa et al., 2004; Caballina et al., 2003; Dhotre and Smith, 2007; Mudde, 2005; Upadhyay et al., 2013). Therefore, even if the air mass flow is kept constant, the void fraction distribution[4] in the impact region may change from one impact test to another, resulting in significant differences of the impact force evolution. Despite this scatter, a general tendency of the impact force to decrease with the average void fraction (or air mass flow rate) is observed. This is clearly visible by considering the force maxima. While the peak force is larger than 70kN for α_0=0% , it decreases to 61kN when α_0=0. 35% and to less than 47kN when α_0=1. 1%.

For each value of α_0, the data from all tests were used to fit to a second-degree polynomial (see Appendix D). The fitting curves for each α_0 are also shown in Fig. 18, and a good agreement with the data is found. This suggests that the impact force is proportional to t^2 in both pure and aerated water, as shown by the numerical simulations. The fitted curves for all values of α_0 are compared in Fig. 19 (the force is plotted as a function of $z-z_0$, with z_0 being the position of the first contact estimated from regression analysis, see Appendix D). This figure makes it clear that, on average, the impact force increases less rapidly with the cone displacement as aeration increases.

From the fitting procedure, an average value of the slamming coefficient f was determined for each initial void fraction (see Appendix D). The obtained results are presented as a function of the initial average void fraction α_0 in Fig. 20-a and as a function of

[4] The inhomogeneity of the instantaneous void fraction discussed here should not be confused with the slight inhomogeneity shown in Fig. 17. Indeed, the results presented in Fig. 17 correspond to average values of the void fraction over the acquisition time (150s). The instantaneous void distribution is probably much more inhomogeneous.

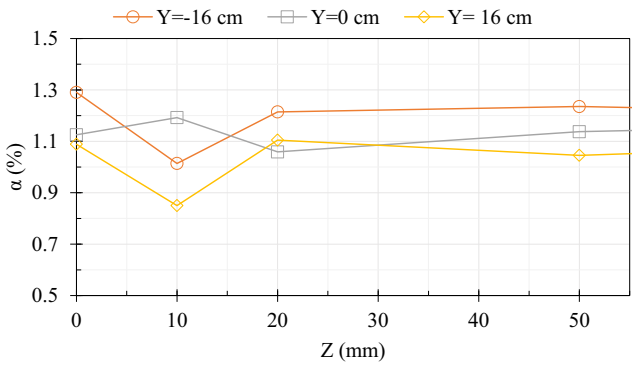

a) Q = 327 Lstd/ min

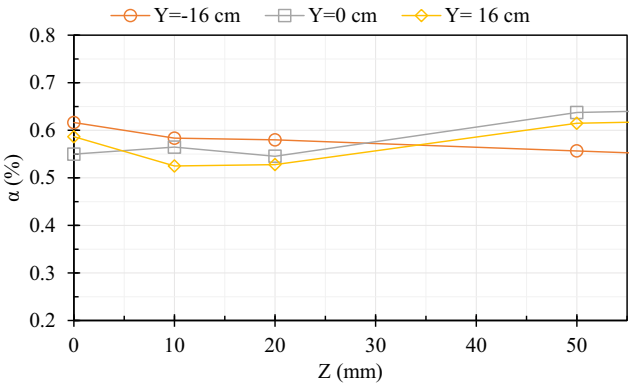

b) Q = 174 .6 Lstd/ min

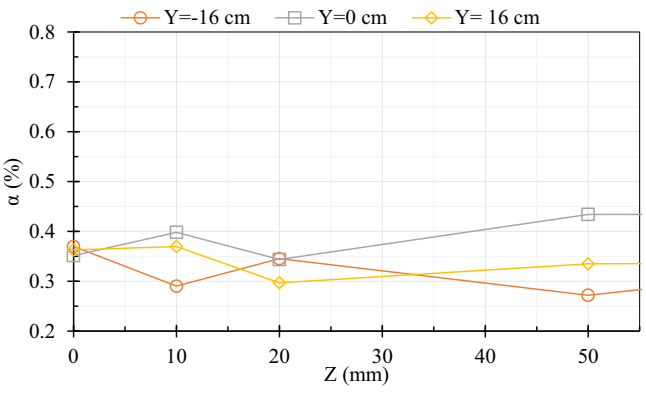

c) Q = 108 .3 Lstd/ min

Fig. 17. Measured void fractions **α** as a function of the vertical position **Z** at three horizontal positions **Y** and for three air mass flow rates **Q**. ***Z = 0*** is the free surface horizontal position and ***Y = 0*** is the horizontal position of the cone axis.

the edge Mach number M in Fig. 20-b (the initial speed of sound in the mixture c_0 was calculated from α_0 using Eq. (10)). It should be noted that the values of M for the tests with aeration are larger than 0. 3 and reach 0. 68 for the largest void fraction. Therefore, these tests are outside the range highlighted in Section 2.3.2 where f is dependent on M only. The slamming coefficient is shown to decrease with the initial void fraction and the Mach number. Indeed, the coefficient f drops from 6.8 for pure water to 5.5 when the

Table 4
Average void fraction α_0 and the corresponding sonic speed c_0 as a function of the air mass flow rate into the aerator.

$Q(L_{std}/min)$	108. 3	174. 6	327
α_0 (%)	0. 35	0. 56	1. 10
c_0 $(m.s^{-1})$	168. 5	133. 6	95. 8

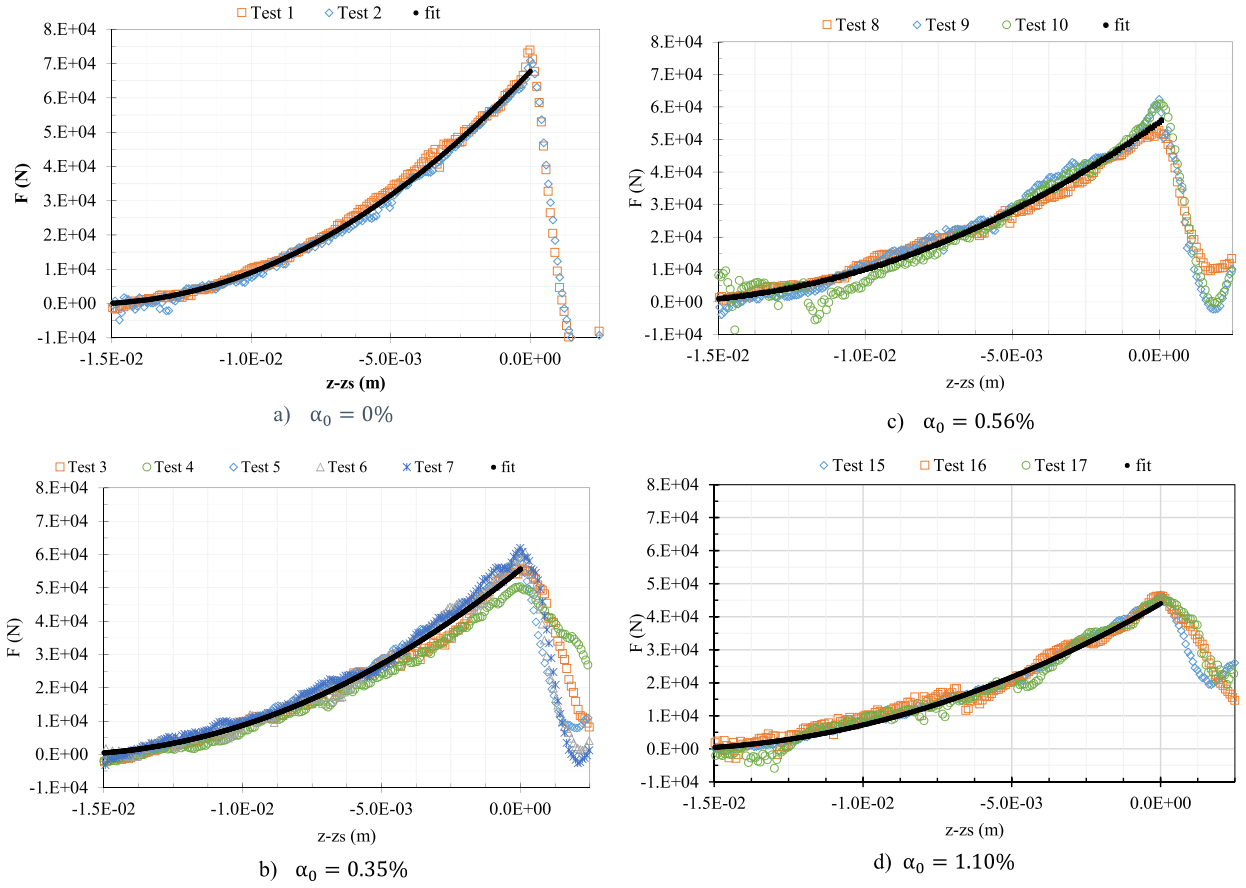

Fig. 18. Evolution of the impact force with the cone displacement from impact tests with several mean void fractions α_0.

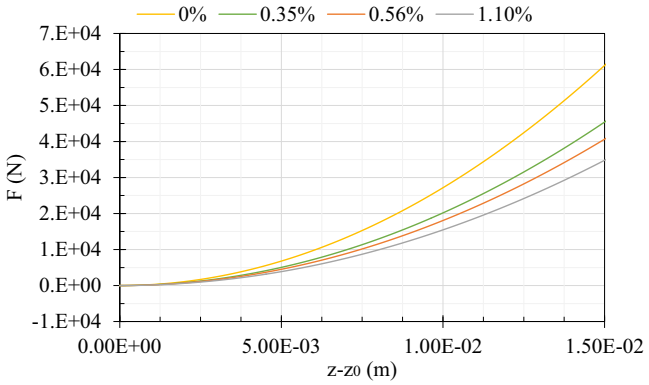

Fig. 19. Comparison of the fitted curves of the impact force **F** (see Fig. 17) as a function of the cone vertical position.

void fraction is α_0=0. 35%. The slamming coefficient is further reduced when the void fraction is α_0=1. 1% where it reaches 4.74, corresponding to a reduction of 30% in comparison with pure water.

Fig. 20 also presents the results of finite element computations carried with the model presented in Section 2. Obviously, the numerical simulations also predict a decrease of the slamming coefficient when the void fraction increases. However, the reduction is less marked than the one observed in experiments. For pure water (α_0=0), the value of f derived from the simulations is in close agreement with the experimental value. For aerated liquids, the numerical model overestimates the slamming coefficient. With α_0=1. 1%, the measured value of f is equal to 4.8, while the modelling predicts a value of 5.8. Several phenomena could be responsible for these differences. First, the numerical model assumes a homogeneous initial void fraction distribution. However, because of the unsteady nature of buoyancy-driven bubbly flows, it is expected that inhomogeneity of the instantaneous void fraction distribution in the impact region exist in experiments. Secondly, it is possible that the motion of the bubbles induces a deformation of the water free surface. These points will deserve attention in the future.

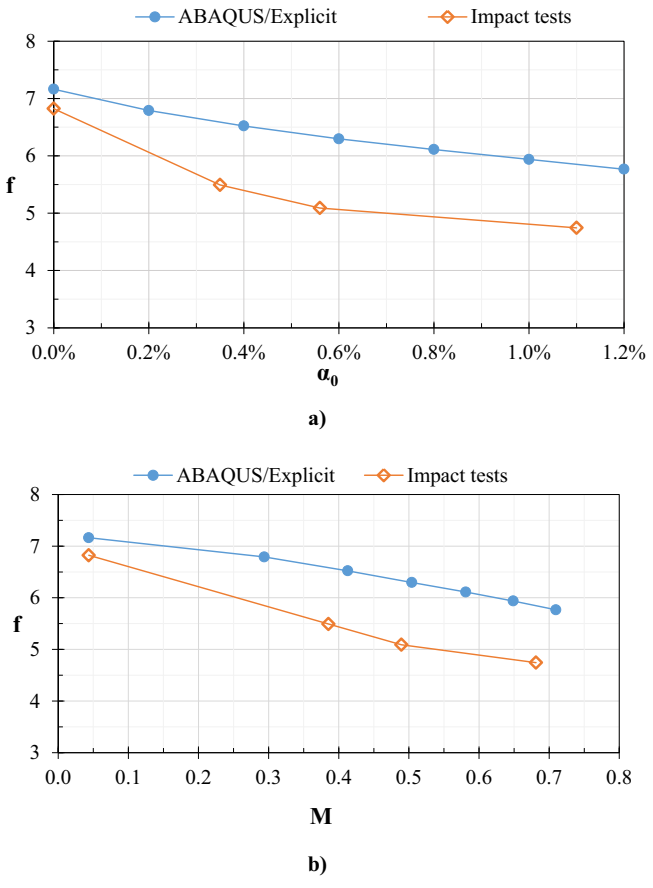

Fig. 20. Slamming coefficients **f** as a function of a) the mean void fraction $\boldsymbol{\alpha_0}$ and b) the Mach number **M**. Blue: numerical results, orange: experimental results. •: numerical results from ABAQUS/Explicit, ◇: experimental results from impact tests

4. Conclusions

In this study, the problem of the impact of a rigid cone upon the surface of aerated water was considered, in order to assess the influence of aeration on slamming loads. The dependence of the impact force on void fraction and impact velocity was investigated by means of finite element simulations for two deadrise angles, 7° and 15° and void fractions of 1%, 5% and 10%.

A significant reduction of the impact force with the increase of the void fraction was highlighted. Reductions of wetted surface and average pressure were also reported. The influence of aeration is dependent on the impact conditions and is the more pronounced when the expansion velocity of the wetted surface is between $100m.s^{-1}$ and $200m.s^{-1}$.

A dimensional analysis was carried out to identify the parameters governing the reduction of the slamming load. Two different ranges were observed, depending on the value of the edge Mach number M (ratio of the expansion velocity of the wetted surface to the initial sonic speed in the bubbly liquid). For $M<0.3$, the slamming coefficient depends only on the Mach number (and not on the initial void fraction). This means that in this range the effect of aeration is mainly related to the decrease of the initial sonic speed with the void fraction. When $M > 0.3$, the slamming coefficient depends on the Mach number **and** on the void fraction. This behaviour is due to the nonlinearity of the equation of state of the air-water mixture. In this case, analytical models of water impact based on the acoustic framework (assuming a constant bulk modulus) are, in their current form, not suitable for the analysis of impacts on aerated liquids.

Experimental impact tests were performed using a hydraulic shock machine and an air-bubble generator. The void fraction distribution was characterized using optical probes. The impact tests were conducted with a cone having a deadrise angle of 7° for an impact velocity of $8m.s^{-1}$ and three average void fractions, 0.35%, 0.56% and 1.1%. The reduction of the impact force and the slamming coefficient due to aeration have been confirmed by these experiments. However, the numerical model seems to overestimate the impact force in the case of aerated water. The conclusions of this study are not restricted to the specific case of cone water entry. They may also be relevant to other solid-liquid impact problems where aeration occurs. This includes breaking wave impacts on breakwaters, where the effect of aeration on the impact pressures and forces is important.

The present study points to several perspectives. First, the attention was mainly focused on global quantities (total force and average pressure). Even if some preliminary results are presented in Section 2.3.1, the influence of aeration on the pressure distribution on the contact surface deserves a more in-depth analysis. Also, it would be interesting to consider impacting bodies with

a more complex geometry, for instance blunt bodies for which the expansion velocity of the surface contact will evolve with time and three-dimensional bodies for which the expansion velocity will vary along the contact line. Some discrepancies between the numerical simulations and the experiments carried out in the present work were observed. In order to understand the origin of these differences, some evolutions of the numerical model are probably required. It is for instance very much likely that the void fraction distribution in experiments is not homogeneous (because of the unsteady nature of bubble plume flows). It would be useful to perform (three-dimensional) simulations with a heterogeneous initial void fraction distribution. Finally, the influence of aeration in engineering problems, like ship slamming, aircraft ditching and wave impact on breakwaters, also deserves some attention.

Acknowledgments

The authors would like to thank all technicians of ENSTA Bretagne for their help in experimental set-up. This work is part of a research programme supported by DGA (French Armaments Procurement Agency). The financial support by Direction Generale de l'Armement (DGA) (Grant n° 2012.60.0010.00.470.75.01) was also greatly appreciated.

Appendix A. Comparison between numerical simulations and the analytical model of Poruchikov (1973)

An analytical model for the impact at constant velocity of a cone on a compressible fluid was proposed by Poruchikov (1973). This model is based on the acoustic theory, i.e. the speed of sound in the liquid is assumed to be constant. Moreover, in Poruchikov's model, the boundary conditions are linearized and imposed on the initial liquid surface (as in the Wagner model). Poruchikov (1973) obtained the following relation that describes the reduction of the slamming coefficient due to compressibility:

$$\frac{f}{f_0} = \left(\frac{\pi}{4}\right)^4 \left(\frac{V_c}{V_e}\right)^4 \tag{A.1}$$

where f_0 is the slamming coefficient at vanishing Mach number. V_c is the expansion velocity of the wetted surface and V_e is the expansion velocity of the intersection circle between the cone and the initial water level (see Eq. (1)). V_c is given by the following equation:

$$\frac{V_c^2}{c_0^2} + \frac{V_c}{c_0}\left(1 - \frac{V_c^2}{c_0^2}\right)^{-1/2} \times \arccos\left(\frac{V_c}{c_0}\right) = 2\frac{V_e}{c_0} \tag{A.2}$$

Fig. A.1 shows a comparison between the predictions of the Poruchikov model and the results of ABAQUS simulations for f/f_0. An excellent agreement is observed between numerical and theoretical results.

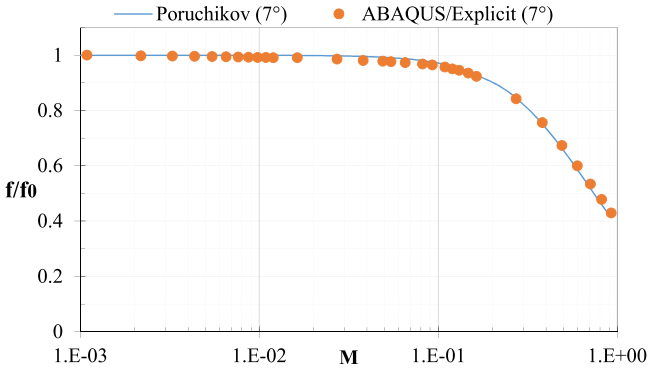

Fig. A.1. Evolution of the slamming coefficient with the Mach number in the case of the impact of a cone with a deadrise angle of 7° on pure water (f_0 is the value of the slamming coefficient for M tending towards to zero). Comparison between the analytical model of Poruchikov (1973) and ABAQUS/explicit simulations.

Appendix B. One-dimensional shock wave propagation in a bubbly mixture

The celerity of a planar shock in a continuum media is given by the following relation (Drumheller, 1998):

$$c_S = \sqrt{\frac{\|T\|}{\rho_0 \|F\|}} \tag{B.1}$$

where $\|T\|$ and $\|F\|$ are respectively the stress and deformation gradient jumps at the shock front. For an inviscid fluid, this equation can be rewritten as:

$$c_S = \sqrt{\frac{P_S - P_0}{\rho_0\left(1 - \frac{v_S}{v_0}\right)}} \tag{B.2}$$

where P_S and $\frac{v_S}{v_0}$ are the pressure and the specific volume behind the shock front. These quantities are linked by the equation of state of the fluid (7).

We carried out simulations of shock propagation in aerated liquids with ABAQUS/Explicit. In these simulations, the domain is rectangular with boundary conditions enforcing a uniaxial deformation state. We used the same mesh size and element type as in the simulations of water impact. Fig. B.1 shows the evolution of the shock celerity c_s as a function of the shock strength P_s for several initial void fractions. The results obtained with ABAQUS are in close agreement with those derived from Eq. (B.2).

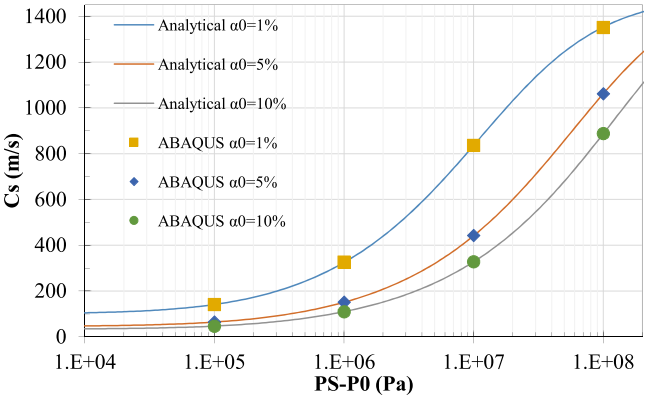

Fig. B.1. Shock celerity c_s in aerated water as a function of the shock strength P_s. Comparison between the analytical solution and simulations carried out with ABAQUS/Explicit.

Appendix C. Derivation of Eq. (8)

The current void fraction in the RVE can be expressed as

$$\alpha = \frac{V_G}{V_G + V_L} \tag{C.1}$$

By dividing the numerator and the denominator by the initial volume of the RVE, this expression can be rewritten in the following form:

$$\alpha = \frac{V_G/V_0}{V_G/V_0 + V_L/V_0} \tag{C.2}$$

By noting that $\frac{V_G}{V_0} = \alpha_0 \frac{V_G}{V_{G0}}$ and $\frac{V_L}{V_0} = (1-\alpha_0)\frac{V_L}{V_{L0}}$, the void fraction can be expressed as a function of the specific volume of the gas and liquid phases:

$$\alpha = \frac{\alpha_0 \frac{V_G}{V_{G0}}}{\alpha_0 \frac{V_G}{V_{G0}} + (1-\alpha_0)\frac{V_L}{V_{L0}}} \tag{C.3}$$

Finally, Eq. (8) is obtained by considering the phase equations of state (5,6).

Appendix D. Curve fitting of the experimental force measurements and determination of an average slamming coefficient

Let z_0 be the vertical position of the cone at the time of the first contact with the liquid free surface and z its position at any time. An alternative expression of the slamming coefficient is:

$$f = \frac{F.\tan^3(\beta)}{\rho_0 V_i^2 (z-z_0)^2} \tag{D.1}$$

By considering the variable

$$Y = \frac{\sqrt{F.\tan^3(\beta)}}{V_i} \tag{D.2}$$

we have the linear relation

$$Y = C_r(z - z_0) \tag{D.3}$$

where

$$C_r = \sqrt{f\rho_0} \tag{D.4}$$

The coefficient C_r and the position z_0 were determined by applying a linear regression analysis. The dependent variable was the values of Y from all tests at the same α_0. The independent variable was the relative position of the cone $z - z_s$ (we considered only the positions before full immersion $z - z_s < 0$, and for which the impact force is larger than 10^4N). The second-degree polynomial best fitting the impact force evolution is therefore:

$$F = \frac{V_i^2}{\tan^3(\beta)} C_r^2 (z - z_0)^2 \tag{D.5}$$

In all cases, the coefficient of determination R^2 of the regression analysis was larger than 0. 9. This shows that the linear model fits fairly well the experimental data, as it explains at least 90% of the variations of the dependent variable Y. The mixture density ρ_0 was computed from α_0 using $\rho_0 = \alpha_0\rho_G + (1-\alpha_0)\rho_L$, and the slamming coefficient f was computed from Eq. (D.4).

Appendix E. Influence of the mesh size

The results presented in the paper were obtained with the mesh described in Section 2.1 that contains 178,648 elements. In order to investigate the influence of the mesh spacing, we also conducted some simulations with a finer mesh that contained 821,144 elements (441,294 4-node elements in the ALE region and 379,850 3-node elements in the Lagrangian region). The two meshes will be referred to as M1 and M2, respectively, in this appendix. The element size in the impact region was equal to 0.25 mm with M1 and to 0.1 mm with M2. It should be noted that M2 leads to much larger CPU times that M1. For instance, a simulation for an impact velocity of 10 m/s, a deadrise rise of 7° and an initial void fraction of 1% lasts 70 min with M1 and more than 20 h with M2 on a Bull R424 cluster equipped with Intel Xeon E5-2670 Processors (2.6 GHz) using 4 cores.

Fig. E.1 presents a comparison of force evolutions obtained with mesh M1 and mesh M2 for several initial void fractions. We

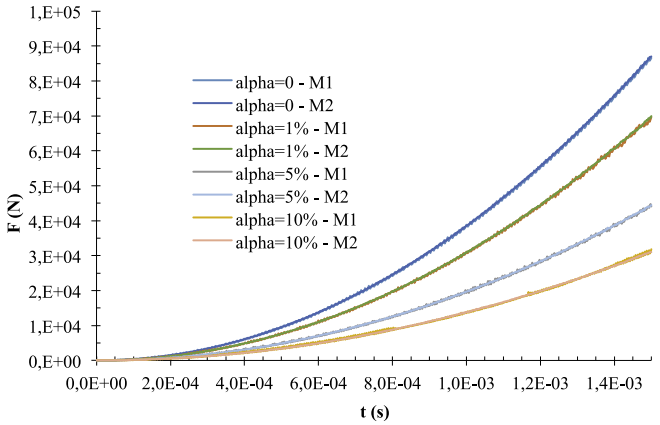

Fig. E.1. Influence of the mesh resolution on the time evolution of the impact force from ABAQUS/Explicit for an impact at 10 m/s of a cone with a deadrise angle of 7°. Four different initial void fractions are considered: α_0=0 (pure water), α_0=1%, α_0=5% and α_0=10%. It is seen that the results obtained with mesh M1 and mesh M2 are almost identical.

Table E.1
Values of the slamming coefficient f (13) corresponding to the curves plotted in Fig. E.1.

α_0	fM1	fM2	Difference
0	7.13	7.16	0.5%
1%	5.77	5.8	0.5%
5%	3.84	3.85	0.3%
10%	2.84	2.85	0.3%

observe that the two meshes provide very close results. The values of the slamming coefficient f (13) corresponding to the curves plotted in Fig. E.1 are given Table E.1. For all void fractions, the difference between the results derived from M1 and M2 is always less than 0.5%.

References

Aquelet, N., Souli, M., Olovsson, L., 2006. Euler-Lagrange coupling with damping effects: application to slamming problems. Comput. Methods Appl. Mech. Eng. 195, 110–132. http://dx.doi.org/10.1016/j.cma.2005.01.010.

Barrau, E., Rivière, N., Poupot, C., Cartellier, A., 1999. Single and double optical probes in air-water two-phase flows: real time signal processing and sensor performance. Int. J. Multiph. Flow. 25, 229–256. http://dx.doi.org/10.1016/S0301-9322(98)00042-1.

Batchelor, G.K., 1967. An Introduction to Fluid Dynamics. Cambridge University Press.

Bredmose, H., Peregrine, D.H., Bullock, G.N., 2009. Violent breaking wave impacts. Part 2: modelling the effect of air. J. Fluid Mech. 641, 389–430. http://dx.doi.org/10.1017/S0022112009991571.

Brennen, C.E., 2005. Fundamentals of Multiphase Flows, Technology. Cambridge University Press. http://dx.doi.org/10.1007/s11214-006-9083-0.

Bullock, G., Crawford, A., Hewson, P., Walkden, M.J., Bird, P.A., 2001. The influence of air and scale on wave impact pressures. Coast. Eng. 42, 291–312. http://dx.doi.org/10.1016/S0378-3839(00)00065-X.

Bullock, G.N., Obhrai, C., Peregrine, D.H., Bredmose, H., 2007. Violent breaking wave impacts. Part 1: results from large-scale regular wave tests on vertical and sloping walls. Coast. Eng. 54, 602–617. http://dx.doi.org/10.1016/j.coastaleng.2006.12.002.

Buwa, V.V., Ranade, V.V., 2004. Characterization of dynamics of gas–liquid flows in rectangular bubble columns. AIChE J. 50 (10), 2394–2407.

Caballina, O., Climent, E., Dušek, J., 2003. Two-way coupling simulations of instabilities in a plane bubble plume. Phys. Fluids 15 (6), 1535–1544.

Carcaterra, A., Ciappi, E., 2000. Prediction of the compressible stage slamming force on rigid and elastic systems impacting on the water surface. Nonlinear Dyn. 21, 193–220.

Carcaterra, A., Ciappi, E., 2004. Hydrodynamic shock of elastic structures impacting on the water: theory and experiments. J. Sound Vib. 271, 411–439. http://dx.doi.org/10.1016/j.jsv.2003.02.005.

Cointe, R., Armand, J.-L., 1987. Hydrodynamic impact analysis of a cylinder. J. Offshore Mech. Arct. Eng. 109, 237–243.

Croci, K., Arrigoni, M., Boyce, P., Gabillet, C., Grandjean, H., Jacques, N., and Kerampran, S. (2014, September). Mitigation of underwater explosion effects by bubble curtains: experiments and modelling. In 23rd MABS (Military Aspects of Blast and Shock), Oxford, UK, 7–12 September, p. 14, 2014.

Dhotre, M.T., Smith, B.L., 2007. CFD simulation of large-scale bubble plumes: comparisons against experiments. Chem. Eng. Sci. 62, 6615–6630. http://dx.doi.org/10.1016/j.ces.2007.08.003.

Dias, F., Dutykh, D., Ghidaglia, J.-M., 2010. A two-fluid model for violent aerated flows. Comput. Fluids 39, 283–293. http://dx.doi.org/10.1016/j.compfluid.2009.09.005.

Drumheller, D.S., 1998. Introduction to Wave Propagation in Nonlinear Fluids and Solids. Cambridge University Press.

El Malki Alaoui, A., Nême, A., Scolan, Y.M., 2015. Experimental investigation of hydrodynamic loads and pressure distribution during a pyramid water entry. J. Fluids Struct. 54, 925–935. http://dx.doi.org/10.1016/j.jfluidstructs.2015.01.018.

El Malki Alaoui, A., Nême, A., Tassin, A., Jacques, N., 2012. Experimental study of coefficients during vertical water entry of axisymmetric rigid shapes at constant speeds. Appl. Ocean Res. 37, 183–197. http://dx.doi.org/10.1016/j.apor.2012.05.007.

Eroshin, V.A., Romanenkov, N.I., Serebryakov, I.V., Yakimov, Y.L., 1980. Hydrodynamic forces produced when blunt bodies strike the surface of a compressible fluide. Fluid Dyn. 15, 829–835.

Eroshin, V.A., Plyusnin, A.V., Romanenkov, N.I., Sozonenko, Y.A., Yakimov, Y.L., 1984. Influence of the atmosphere on the magnitude of the hydrodynamic forces in the case of a disk in a flat encounter with the surface of a compressible liquid. Fluid Dyn. 19. http://dx.doi.org/10.1007/BF01093895.

Eroshin, V.A., Konstantinov, G.A., Romanenkov, N.I., Yakimov, Y.L., 1988. Experimental determination of the pressure on a disk entering a compressible fluid at an angle to the free surface. Fluid Dyn. 23. http://dx.doi.org/10.1007/BF01051884.

Federico, F., Amoruso, A., 2009. Impact between fluids and solids. Comparison between analytical and FEA results. Int. J. Impact Eng. 36, 154–164. http://dx.doi.org/10.1016/j.ijimpeng.2007.11.005.

Grandjean, H., Jacques, N., Zaleski, S., 2012. Shock propagation in liquids containing bubbly clusters: a continuum approach. J. Fluid Mech. 701, 304–332. http://dx.doi.org/10.1017/jfm.2012.159.

Hattori, M., Arami, A., Yui, T., 1994. Wave impact pressure on vertical walls under breaking waves of various types. Coast. Eng. 22, 79–114. http://dx.doi.org/10.1016/0378-3839(94)90049-3.

Jacques, N., Constantinescu, A., Kerampran, S., Nême, A., 2010. Comparaison de différentes approaches pour la simulation numérique d'impacts hydrodynamiques. Eur. J. Comput. Mech. Eur. Mécanique Numér. 19, 743–770. http://dx.doi.org/10.3166/ejcm.19.743-770.

Kameda, M., Shimaura, N., Higashino, F., Matsumoto, Y., 1998. Shock waves in a uniform bubbly flow. Phys. Fluids 10 (10), 2661–2668.

Kapsenberg, G.K., 2011. Slamming of ships: where are we now? Philos. Trans. A. Math. Phys. Eng. Sci. 369, 2892–2919. http://dx.doi.org/10.1098/rsta.2011.0118.

Korobkin, A., 1992. Blunt-body impact on a compressible liquid surface. J. Fluid Mech. 244, 437–453.

Korobkin, A., 1994. Blunt-body impact on the free surface of a compressible liquid. J. Fluid Mech. 263, 319–342. http://dx.doi.org/10.1017/S0022112094004131.

Korobkin, A., 2004. Analytical models of water impact. Eur. J. Appl. Math. 15 (06), 821–838.

Korobkin, A., Malenica, S., 2016. Rational assessment of fluid impact loads. In: Aston, J.P., Mulholland, J.A., Tant, M.M.K. (Eds.), UK Success Stories in Industrial Mathematics. Springer International Publishing, Cham, 99–105. http://dx.doi.org/10.1007/978-3-319-25454-8_13.

Kubenko, V.D., Gavrinlenko, V.V., 1986. Penetration of a compressible liquid by an axially symmetric solid object. Transl. Prikl. Mekhanika 22, 93–99.

Kubenko, V.D., Gavrinlenko, V.V., 1987. Axisymmetric problem of the penetration of rigid bodies into a compressible liquid. Transl. Prikl. Mekhanika 23, 53–60.

Mäkiharju, S.A., Gabillet, C., Paik, B.-G., Chang, N.A., Perlin, M., Ceccio, S.L., 2013. Time-resolved two-dimensional X-ray densitometry of a two-phase flow downstream of a ventilated cavity. Exp. Fluids 54, 1561. http://dx.doi.org/10.1007/s00348-013-1561-z.

Mudde, R.F., 2005. Gravity-driven bubbly flows. Annu. Rev. Fluid Mech. 37, 393–423.

Peregrine, D.H., Thais, L., 1996. The effect of entrained air in violent water wave impacts. J. Fluid Mech. 325, 377–397.

Peseux, B., Gornet, L., Donguy, B., 2005. Hydrodynamic impact: numerical and experimental investigations. J. Fluids Struct. 21, 277–303. http://dx.doi.org/10.1016/j.jfluidstructs.2005.04.011.

Poruchikov, V.B., 1973. Penetration of a cone into a compressible fluid. J. Appl. Math. Mech. 37, 74–83. http://dx.doi.org/10.1016/0021-8928(73)90137-8.

Poruchikov, V.B., 1974. Entry of a wedge into a compressible liquid. Fluid Dyn. 9 (2), 293–296. http://dx.doi.org/10.1007/BF01092666.

Seddon, C.M., Moatamedi, M., 2006. Review of water entry with applications to aerospace structures. Int. J. Impact Eng. 32, 1045–1067. http://dx.doi.org/10.1016/j.ijimpeng.2004.09.002.

Shiffman, M., Spencer, D.C., 1951. The force of impact on a cone striking a water surface (vertical entry). Commun. Pure Appl. Math. 4, 379–417. http://dx.doi.org/10.1002/cpa.3160040402.

Skalak, R., Feit, D., 1966. Impact on the surface of a compressible fluid. J. Manuf. Sci. Eng. 88, 325–331.

Souli, M., Ouahsine, A., Lewin, L., 2000. ALE formulation for fluid–structure interaction problems. Comput. Methods Appl. Mech. Eng. 190 (5), 659–675.

Tassin, A., Korobkin, A.A., Cooker, M.J., 2014. On analytical models of vertical water entry of a symmetric body with separation and cavity initiation. Appl. Ocean Res. 48, 33–41.

Tassin, A., Jacques, N., El Malki Alaoui, A., Nême, A., Leblé, B., 2010. Assessment and comparison of several analytical models of water impact. Int. J. Multiphys. 4, 125–140.

Tassin, A., Jacques, N., El Malki Alaoui, A., Nême, A., Leblé, B., 2012. Hydrodynamic loads during water impact of three-dimensional solids: modelling and experiments. J. Fluids Struct. 28, 211–231. http://dx.doi.org/10.1016/j.jfluidstructs.2011.06.012.

Upadhyay, R.K., Pant, H.J., Roy, S., 2013. Liquid flow patterns in rectangular air-water bubble column investigated with radioactive particle tracking. Chem. Eng. Sci. 96, 152–164.

van Wijngaarden, L., 1972. One-dimensional flow of liquids containing small gas bubbles. Annu. Rev. Fluid Mech.. http://dx.doi.org/10.1146/annurev.fl.04.010172.002101.
von Karman, T.V., 1929. The Impact on Seaplane Floats During Landing.
Wagner, H., 1932. Über Stoß- und Gleitvorgänge an der Oberfläche von Flüssigkeiten. J. Appl. Math. Mech. / Z. für Angew. Math. und Mech. 12, 193–215.
Walkden, A., 1999. Model Wave Impulse Loads on Caisson Breakwaters: Aeration, Scale and Structural Response. University of Plymouth, Plymouth,UK.
Wang, S., Guedes Soares, C., 2014. Numerical study on the water impact of 3D bodies by an explicit finite element method. Ocean Eng. 78, 73–88. http://dx.doi.org/10.1016/j.oceaneng.2013.12.008.
Watanabe, M., Prosperetti, A., 1994. Shock waves in dilute bubbly liquids. J. Fluid Mech. 274, 349–381. http://dx.doi.org/10.1017/S0022112094002156.
Wilson, W.D., 1959. Speed of sound in distilled water as a function of temperature and pressure. J. Acoust. Soc. Am. 31 (8), 1067–1072.
Zhao, R., Faltinsen, O., 1993. Water entry of two-dimensional bodies. J. Fluid Mech. 246, 593–612. http://dx.doi.org/10.1017/S002211209300028X.